crystals

MDPI

Article

Strain-Induced Band Gap Variation in InGaN/GaN Short Period Superlattices

Polyxeni Chatzopoulou [1], Isaak G. Vasileiadis [1], Philomela Komninou [1], Vassilis Pontikis [2], Theodoros Karakostas [1] and George P. Dimitrakopulos [1,*]

[1] School of Physics, Aristotle University of Thessaloniki, GR 54124 Thessaloniki, Greece; pochatzo@physics.auth.gr (P.C.); isvasile@physics.auth.gr (I.G.V.); komnhnoy@auth.gr (P.K.); karakost@auth.gr (T.K.)

[2] DRF/IRAMIS, Centre d'Etudes de Saclay, Commissariat à l'Energie Atomique et aux Energies Alternatives, Université Paris-Saclay, 91191 Gif-sur-Yvette, France; vassilis.pontikis@cea.fr

* Correspondence: gdim@auth.gr

Abstract: The use of strained substrates may overcome indium incorporation limits without inducing plastic relaxation in InGaN quantum wells, and this is particularly important for short-period InGaN/GaN superlattices. By incorporating elastic strain into these heterostructures, their optoelectronic behavior is modified. Our study employed density functional theory calculations to investigate the variation in the band-gap energy of short-period InGaN/GaN superlattices that comprise pseudomorphic quantum wells with a thickness of just one monolayer. Heterostructures with equibiaxially strained GaN barriers were compared with respective ones with relaxed barriers. The findings reveal a reduction of the band gap for lower indium contents, which is attributed to the influence of the highly strained nitrogen sublattice. However, above mid-range indium compositions, the situation is reversed, and the band gap increases with the indium content. This phenomenon is attributed to the reduction of the compressive strain in the quantum wells caused by the tensile strain of the barriers. Our study also considered local indium clustering induced by phase separation as another possible modifier of the band gap. However, unlike the substrate-controlled strain, this was not found to exert a significant influence on the band gap. Overall, this study provides important insights into the behavior of the band-gap energy of strained superlattices toward optimizing the performance of optoelectronic devices based on InGaN/GaN heterostructures.

Keywords: InGaN; quantum wells; strain; band gap; DFT; III-nitrides; superlattices

Citation: Chatzopoulou, P.; Vasileiadis, I.G.; Komninou, P.; Pontikis, V.; Karakostas, T.; Dimitrakopulos, G.P. Strain-Induced Band Gap Variation in InGaN/GaN Short Period Superlattices. *Crystals* **2023**, *13*, 700. https://doi.org/10.3390/cryst13040700

Academic Editor: Ray-Hua Horng

Received: 28 March 2023
Revised: 13 April 2023
Accepted: 17 April 2023
Published: 19 April 2023

1. Introduction

Ultra-thin $In_xGa_{1-x}N$/GaN quantum wells have concentrated significant interest for use in band-gap engineering [1–5]. Such quantum wells can, in principle, accommodate a high indium content while remaining pseudomorphic. In addition, the extremely small quantum well thickness would minimize the quantum-confined Stark effect [6]. Multi-quantum wells can be employed to compose short-period superlattices and even form digital alloys with unique properties [3]. Moreover, theoretical calculations suggest that such superlattices can exhibit topological insulator behavior as indicated by a high electron gas mobility observed experimentally [7–9].

Ultra-thin (0001)-oriented $In_xGa_{1-x}N$/GaN quantum wells with thicknesses from one up to two monolayers (whereby one monolayer is one (0002) lattice plane of the wurtzite crystal structure and comprises both metal and nitrogen atoms—see Figure 1a) have been deposited by plasma-assisted molecular beam epitaxy by combining excessively high indium fluxes with growth temperatures exceeding the decomposition temperature of InN [10,11]. However, the experimentally achieved indium content has been lower than the intended x = 100% (i.e., binary InN) [12–15]. A model comprising InN islands was suggested, which could attribute this lower indium content to an averaging effect,

as it was claimed that InN is stabilized by a host-matrix strengthening effect [16]. This stabilization was attributed to the nitrogen atoms directly below the indium atoms being strongly bonded to gallium atoms (0.39 eV/bond difference in cohesive energies between Ga–N and In–N bonds). By considering the growth of an InN monolayer on the (0001) GaN surface, the nitrogen atoms of the monolayer share three bonds with indium atoms and one bond with a gallium atom. In contrast, nitrogen atoms in InN form four bonds with indium atoms. Hence, the InN monolayer is more strongly bound to the GaN surface and more stable at higher temperatures in comparison with it being inside an InN epilayer. However, we have shown that this effect cannot stabilize the deposition of a binary InN layer [17]. For deposition under effective N-rich conditions, it was shown that an ordered quantum well structure of just x = 25% can be stabilized [18]. For metal-rich conditions, we have suggested a growth model based on experimental observations whereby, above the InN decomposition temperature, a single $In_xGa_{1-x}N$ monolayer is stabilized through a substitutional synthesis mechanism involving the exchange between In and Ga atoms [17]. Using this mechanism, we have achieved an indium content of x = ~45%, which is the highest reported so far.

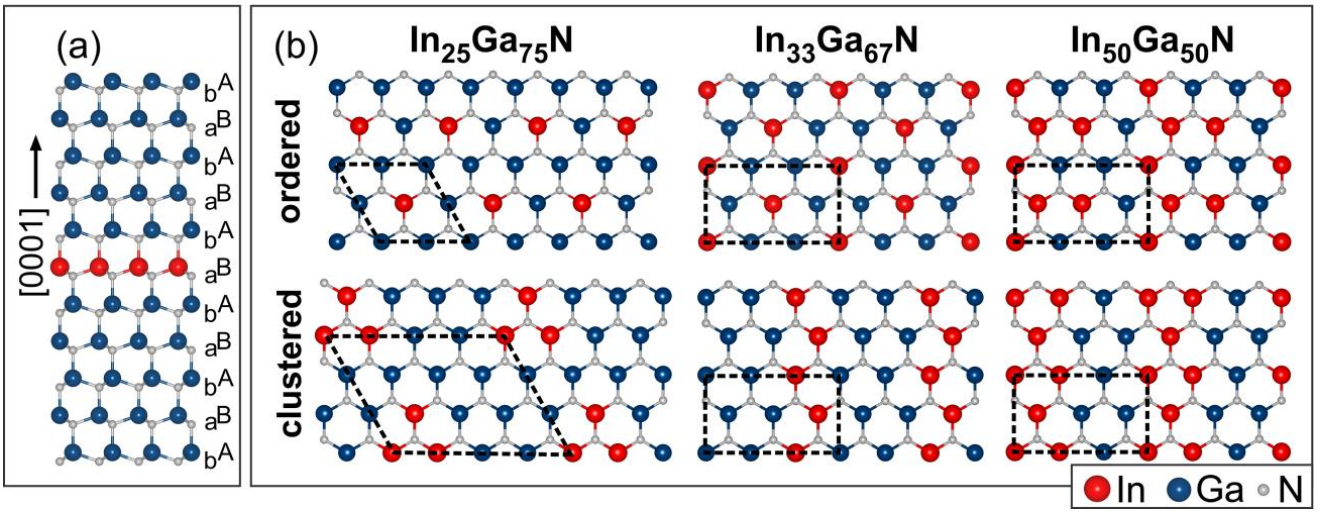

Figure 1. (**a**) Cross-sectional schematic illustration of InN quantum well with one monolayer thickness in (0001)-oriented GaN barriers (projection along $[11\bar{2}0]$). The monolayer can be bA or aB. The material is shown with metal polarity consistent with experimental growths. (**b**) Plan-view illustrations of ordered and clustered configurations of (0002) $In_xGa_{1-x}N$ monolayers, for structures up to indium content of x = 50%. Higher compositions of 67% and 75% can be obtained from the respective 33% and 25% ones by the interchange of indium with gallium atoms.

Reducing the lattice misfit between quantum well and barriers is a critical factor for increasing the indium content without plastic relaxation [19–22]. It has been shown that an increase in the GaN lattice parameter by 2% can induce up to a threefold increase in indium incorporation in $In_xGa_{1-x}N$ quantum wells [23]. Efforts are, therefore, underway to reduce the misfit. However, for the efficient deployment of this approach, a theoretical understanding of the dependence of the superlattice's band-gap energy on the strain that is imposed on the heterostructure is required. Another issue pertains to the influence on the band gap of a possible compositional inhomogeneity of the $In_xGa_{1-x}N$ quantum wells due to local phase separation into InN and GaN [24]. This relates to the suggestion regarding an inhomogeneous distribution of the indium content [16]. Toward these aims, we have performed density functional theory (DFT) calculations of monolayer-thick $In_xGa_{1-x}N$ quantum wells on strained barriers, as well as calculations of phase-separated monolayer-thick quantum wells. We have thus obtained the band-gap variation across the compositional range up to x = 100% indium content and correlated this with the strain state of the short-period

superlattices. The results provide an understanding of the compositional range for which the deployment of strained barriers is effective in reducing the band gap of the superlattice and elucidate the influence of clustering.

2. Computational Method and Details

The energetic and structural characteristics of the short-period superlattices were investigated using the Quantum Espresso ab initio package [25,26] employing exchange correlation energy functionals with local density approximation with modified pseudopotentials (MPP-LDA) [27]. This method comprises the estimation of both the structural and electronic properties (energy gaps and densities of states—DOS) with good agreement to their experimental values. The calculations were made with the Broyden–Fletcher–Goldfarb–Shanno minimization algorithm [28], and cutoffs were set at E_c = 140 Ry for the kinetic energy of plane waves and r_c = 560 Ry for the charge density. The following convergence criteria were used: $\delta E < 10^{-10}$ Ry for energy, $\delta F < 10^{-10}$ Ry/Bohr for forces, and $\delta\sigma < 10^{-10}$ kbar for stress.

Preliminary DFT calculations were first performed on the supercells of bulk $In_xGa_{1-x}N$ alloys of various compositions. Calculated equilibrium lattice parameters were compliant to Vegard's law, while the band-gap bowing parameter was determined at $b = 1.18 \pm 0.09$ eV, in good agreement with theoretical and experimental reports [29,30] (see supplementary material, Figures S1 and S2). Moreover, DFT calculations were performed to generate the band structure of strain-free and strained GaN and InN with the wurtzite crystal structure. A biaxial stress state (tetragonal distortion) was applied with imposed equibiaxial in-plane strain of up to ±5% (tensile for GaN and compressive for InN). In both cases, a reduction of the band gap due to the strain was observed. The determined band gaps and band structures were consistent with the literature [31,32]. In GaN, the band-gap energy reduced from 3.28 eV for relaxed to 2.65 eV for +5% strain. In InN, the band gap changed from 0.85 for relaxed to 0.69 eV for −5% strain.

Initially, we performed anisotropic elasticity calculations using Fischer's model [33] to determine the critical thickness of (0001)-oriented wurtzite GaN and found that it reduces to less than 10 monolayers if the strain on the basal plane exceeds 4% (see supplementary material, Figure S3a). Therefore, our (0001) superlattice supercells were constructed by taking GaN barriers strained by less than 4%, i.e., 0% (no strain), 1.5%, and 3%, and by choosing a GaN barrier thickness of seven monolayers. Hence, the employed superlattice periodicity in our calculations was $1In_xGa_{1-x}N/7GaN$ for all cases. To ensure the generality of our results, we also verified that the band gap of the superlattice heterostructure remains constant if the GaN barrier thickness is greater than seven monolayers, i.e., for elastically strained $1In_xGa_{1-x}N/nGaN$ heterostructures with $n \geq 7$. This is illustrated in supplementary material Figure S3b and is consistent with the results of Ref. [34].

The employed methodological approach of this work is illustrated in the block diagram of Figure 2. Following the aforementioned preliminary calculations, we considered the influences of GaN barrier strain and indium clustering. The outputs of the DFT analysis were the DOS, band-gap energies, strain, and formation energies. Band structure analysis was not in the scope of this work. Using the extracted results, we correlated the indium composition with the excess energy of the supercells and with the change in the band-gap energy relative to the unstrained (0%) supercells. Calculations were performed across the whole compositional range.

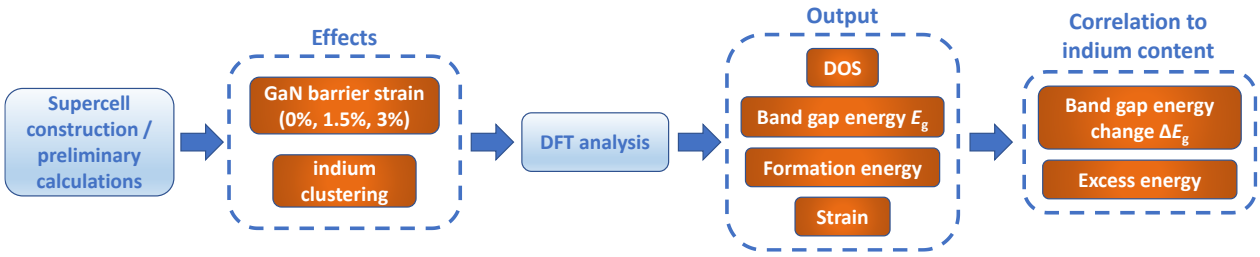

Figure 2. Block diagram illustrating the adopted methodological approach for studying influences of strain and clustering, and correlation of the results to the indium content of quantum wells.

3. Results and Discussion

Using the aforementioned superlattice periodicity, our calculations first considered quantum wells with ordered distributions of indium atoms. Such quantum wells had indium contents spanning the whole compositional range from $x = 0$ to 100% (binary InN). The employed ordered configurations of 25%, 33%, 50%, 67%, and 75% are illustrated in Figure 1b. In addition to the ordered indium configurations, we also considered quantum wells that were phase-separated into InN and GaN clusters. Such quantum well heterostructures were calculated in order to appreciate the influence of clustering on the band gap. Previous calculations have shown that indium clustering can impose a small band-gap reduction [1,35]. The employed configurations are also given in Figure 1b. Clustering can, of course, be realized in different ways by varying the supercell geometry or period. We considered clustering of the minority cations on a corner or side of the InGaN monolayer. An additional constraint was the need to maintain a periodic supercell. We kept the same size of the supercells between uniform and clustered cases except for the 25% and 75% cases where the ordered supercells were too small, containing just one minority cation, and hence the size had to be increased for the clustered cases. These calculations of phase-separated $In_xGa_{1-x}N$ quantum wells were performed only for relaxed GaN barriers.

Following supercell construction, the densities of states were calculated for all the configurations. Figure 3a–c illustrate partial DOS diagrams for bulk GaN and for short-period superlattices comprising quantum wells with 50% and 100% indium content. The partial DOS diagrams are illustrated for the in-plane strains of 0% and 3% and for each chemical element separately. Figure 3d–f show the respective total DOS diagrams. For GaN, Figure 3a,d demonstrate the reduction of the band gap due to the strain. This is manifested by the relative displacements between the DOS plots for relaxed and strained GaN. This reduction is more pronounced for the case of the nitrogen sublattice. However, as seen in Figure 3d–f, this strain-induced band-gap reduction gradually diminishes with increasing indium content. For higher indium contents, such as for InN quantum wells, there is even a reversal, i.e., the band gap appears to increase back up.

Figure 4a summarizes the band-gap variation of the short-period superlattice heterostructures with increasing indium content. It is seen that, for low indium contents, the band-gap energy reduction is larger for the higher strains. In Figure 4a, the vertical line indicates the highest indium content experimentally reported so far, which has been achieved for one-monolayer quantum wells deposited on relaxed GaN [17]. For quantum wells with indium contents in this compositional range, it can be seen that the strain has a rather minor influence on the band gap. In fact, there is a crossover point in the range of $x = 50$–70%, after which the strain increases the band gap of the superlattice instead of reducing it.

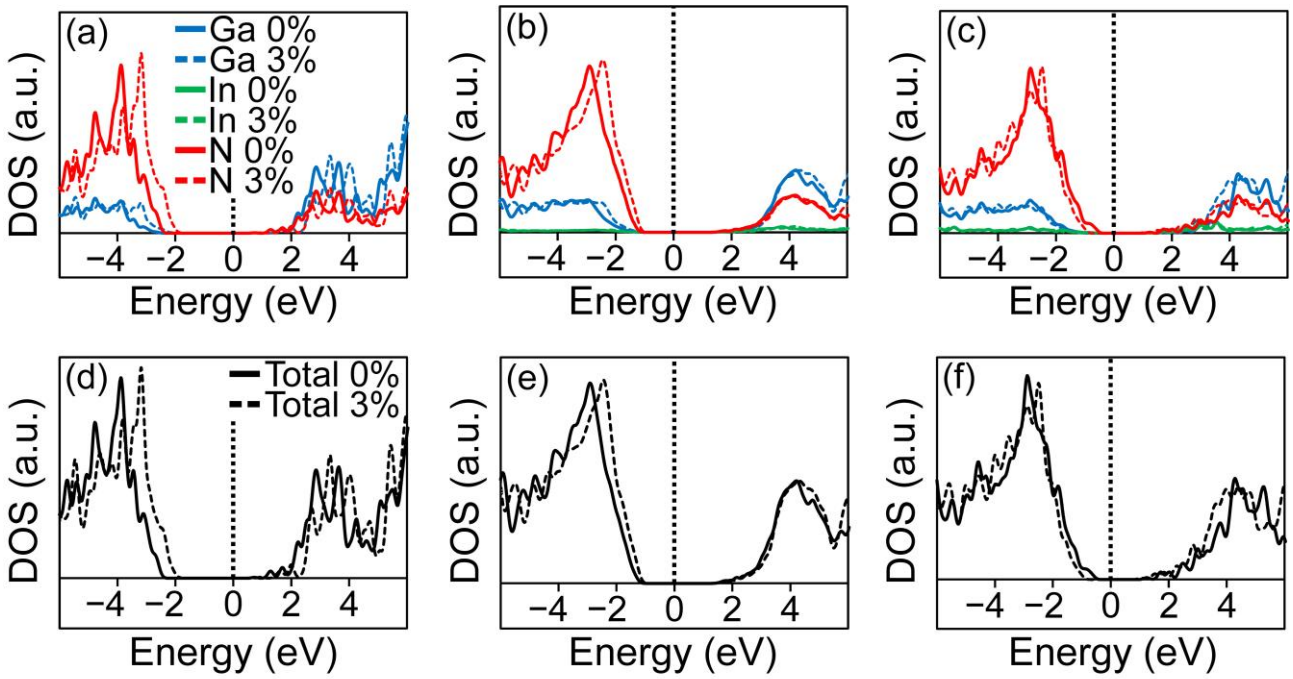

Figure 3. Partial DOS diagrams for each element (**top**, colored diagrams) and total ones (**bottom** diagrams) obtained from relaxed and 3% strained short-period superlattices. (**a**,**d**) Binary GaN; (**b**,**e**) superlattices with $In_{0.5}Ga_{0.5}N$ quantum wells; and (**c**,**f**) superlattices with InN quantum wells.

If we compare this trend with that of the bulk GaN and InN binaries under a similar strain state, we find an analogy as shown in the inset of Figure 4a. When a tensile biaxial stress state is imposed on GaN, its band gap is reduced, and this is shown in the inset of Figure 4a for 1.5% and 3% in-plane strain. Regarding InN, the inset of Figure 4a shows its band-gap variation when it is compressively strained to match the in-plane lattice constant of GaN. For InN pseudomorphic on relaxed GaN (−9.5% in-plane strain), its band gap is also reduced since both the compressive and tensile strain tend to reduce the band gap. However, if InN is pseudomorphic to tensily strained GaN, then the compressive strain of InN is reduced compared with the previous case to −8.2% for +1.5% strained GaN and to −6.8% for +3% strained GaN. As a result, the band gap of InN on strained GaN increases back up.

This reversal is better illustrated in Figure 4b, which shows that, for the superlattice heterostructures, the change ΔE_g of the band-gap energy compared with heterostructures with relaxed GaN barriers becomes positive for higher indium contents. The rate of change is steeper for the 3% strain compared with that for 1.5%. The linear equations are $\Delta E_g(1.5\%) = 2.9 \times 10^{-3}x - 0.16$ and $\Delta E_g(3\%) = 5.9 \times 10^{-3}x - 0.39$. We observe that $\Delta E_g(3\%)/\Delta E_g(1.5\%) \cong 2$, i.e., about equal to the ratio of the strains. Overall, although tensile-strained GaN can aid the incorporation of indium [23], our calculations reveal that this approach toward band-gap reduction is useful only for low indium contents. In fact, such contents, in the range up to x = ~45%, are experimentally also attainable without strained GaN barriers. The regions of negative and positive variations of ΔE_g with composition and barrier strain are schematically illustrated in the contour plot in Figure 4c.

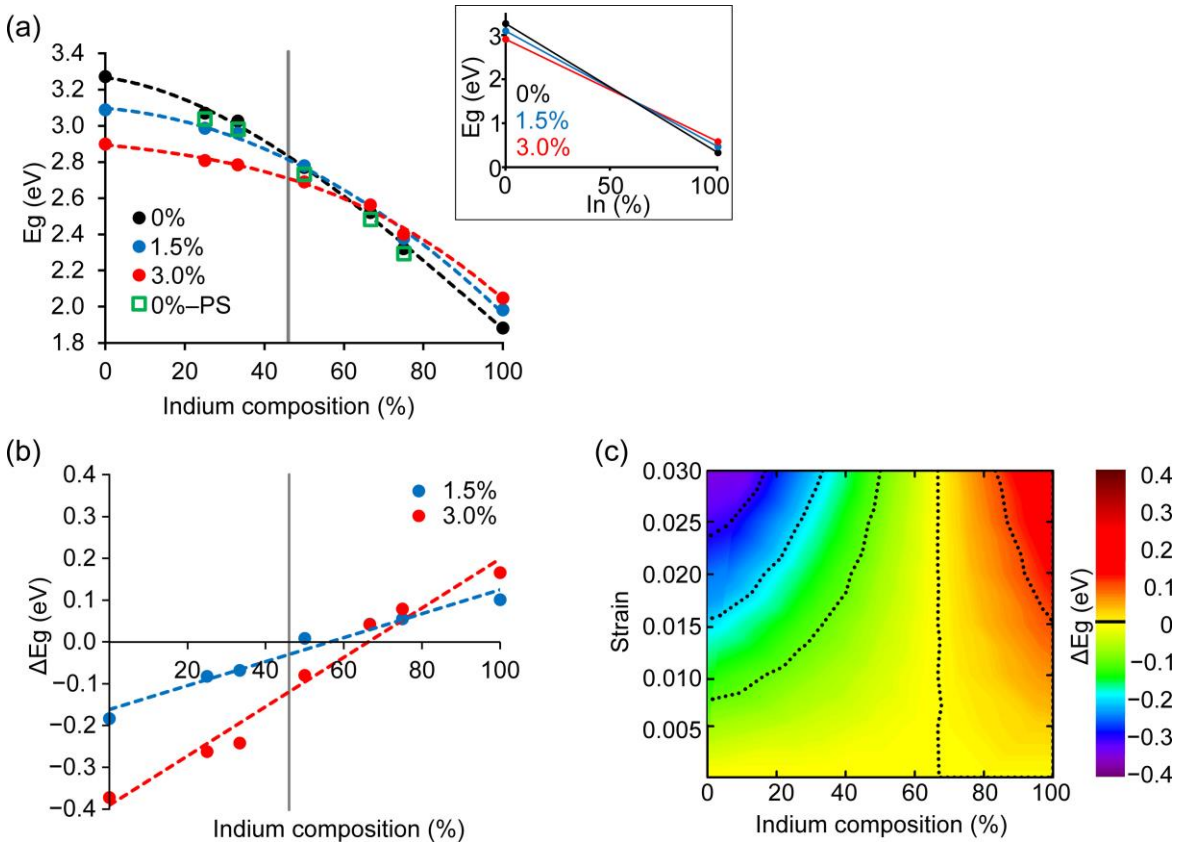

Figure 4. (**a**) Diagram of band-gap energy of short-period superlattice with respect to the indium content of its quantum wells. Vertical gray line indicates the highest indium content experimentally achieved so far. PS indicates heterostructures with phase-separated quantum wells. Inset illustrates band gaps of bulk GaN, relaxed and equibiaxially strained on the basal plane, and of bulk InN when pseudomorphic to relaxed or strained GaN. (**b**) Diagram of band-gap energy change ΔE_g with respect to relaxed GaN plotted against indium content. Change from negative to positive values is observed after 50–70% indium content. (**c**) Contour plot showing variation of ΔE_g depending on composition of quantum well and strain in the barrier.

Regarding the influence of phase separation leading to InN clustering, our calculations over the whole compositional range show that the phase-separated quantum wells exhibit a behavior that is similar to the respective homogeneous ones and induce only a small reduction in the band gap, as can be seen in Figure 4a. The largest reduction is observed for the 33% indium case, which amounts to 0.04 eV. The small influence is attributed to the small amount of the alloying element in the supercell, as well as to the negligible influence of the clustering in changing the strain of the supercell compared with the ordered or disordered cases, as illustrated in supplementary material Figure S4. Hence, the experimental formation of local InN clusters would not lead to any appreciable change in the band gap. It also would not be easily discernible by high-resolution scanning–transmission electron microscopy (HRSTEM) since in cross-sectional observations the projections of such regions overlap and thereby prevent resolving this issue experimentally.

Following the determination of the band-gap variation, we considered its correlation to the strain distribution in the short-period superlattices. Figure 5a,b illustrate representative distributions of the interplanar *d*-spacing of (0002) planes for the metal and nitrogen sublattices, respectively. In the case of $In_xGa_{1-x}N$ quantum wells, there are, of course, slight variations in the bond lengths depending on whether the quantum well atom is Ga or In, and we define the position of the (0002) atomic plane by the average of atomic positions along [0001]. For each atomic plane, the graphs of Figure 5a,b give the *d*-spacing with the

former plane, i.e., the plane below it along the [0001] direction. The indium-rich quantum well plane is the 6th one in the stacking sequence, as indicated by the arrow in Figure 5. The *d*-spacing distributions are illustrated for representative $In_xGa_{1-x}N$ quantum wells with x = 50% and 100% and for relaxed and 3%-strained GaN barriers. It is straightforward to see that the nitrogen sublattice is much more affected regarding the change in the *d*-spacing. On the other hand, only one *d*-spacing is affected for the nitrogen sublattice (i.e., the one illustrated in Figure 5b), compared with two *d*-spacings (on either side of the monolayer) for the metal sublattice. The reduced relative variations of the *d*-spacings with respect to those of the GaN barriers are almost identical for quantum wells on strained or relaxed barriers. For the nitrogen sublattice, this is approximately double that of the metal sublattice. As indicated in Figure 5b, the *d*-spacing above the quantum well is smaller by ~0.06 Å in the case of the superlattice with 3%-strained barriers. On the other hand, the internal parameter u of the wurtzite structure locally increases as shown in Figure 5c. Therefore, this reduction of the *d*-spacing is attributed to the parameter $t = d - u$, which is reduced by ~0.08 Å as shown in Figure 5d. This means that the $In_xGa_{1-x}N$ monolayer is less strained when deposited on strained GaN, resulting in a smaller band-gap reduction for the whole superlattice heterostructure than what would be expected simply on account of the increase in the quantum well indium content.

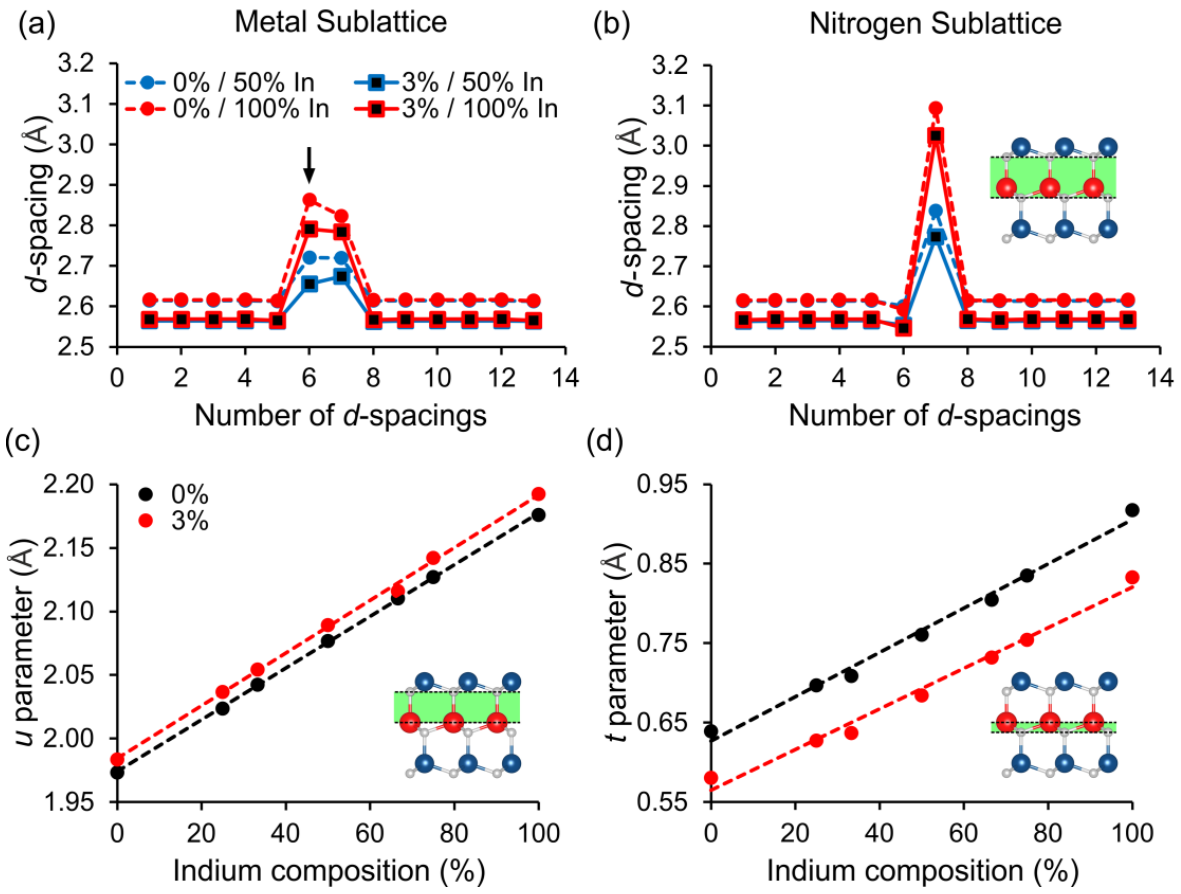

Figure 5. (**a**,**b**) Profiles along [0001] of *d*-spacing of metal and nitrogen (0002) planes for 1-monolayer $In_xGa_{1-x}N$ quantum wells, respectively. Cases with relaxed and 3%-strained GaN barriers are given. The arrow indicates the position of monolayer quantum well. (**c**,**d**) Graphs with respect to composition of local internal parameter u of wurtzite structure and parameter $t = d - u$, respectively. Illustrated parameters u and t add up to yield the maximum *d*-spacing of nitrogen planes of the quantum well as schematically shown in the insets.

For relaxed GaN barriers, theoretically acquired profiles were verified against experimental observations obtained by probe-corrected HRSTEM from $In_xGa_{1-x}N$/GaN superlattices with one-monolayer quantum wells, as detailed elsewhere [17]. Figure 6a illustrates an HRSTEM image of a $In_xGa_{1-x}N$ quantum well with composition close to x = 30%. In Figure 6b, the theoretical strain distribution for the given indium content is overlapped on the corresponding experimental profile. The latter was obtained by using the methodology of Voronoi tessellation of the experimental image around the positions of projected atomic columns that were determined by peak finding. This method allows for the measurement of the *c*-lattice constant, i.e., the strain is defined with respect to the relaxed unit cell constant of GaN. The projected intensity of atomic columns was quantified as Z-contrast using comparison with multislice image simulations under the frozen phonon approximation and was directly interpreted as indium composition. Therefore, both the strain and compositional profiles were experimentally attainable. The lattice strain depicted in Figure 6b is defined as $e_{zz} = (c - c_{GaN})/c_{GaN}$, i.e., as the reduced relative variation of the *c*-lattice constant along [0001]. In this equation, we assign to each atomic plane the *c*-spacing below it, similar to what was adopted in Figure 5 for the *d*-spacings. The respective theoretical strain profiles superimposed in Figure 6b correspond to the metal and nitrogen sublattices for x = 33%. Excellent matching is observed between the experimental and theoretical profiles for the metal sublattice. This is normal since the experimental positions of projected atomic columns are more influenced by the metal sublattice due to its much higher atomic number. The maximum values of the lattice strain in both sublattices are almost equal despite the much larger variation of the local *d*-spacing in the case of the nitrogen sublattice that is depicted in Figure 5b. This is because this local change affects two successive *c*-lattice constants along [0001]. As shown in Figure 5a,b, the metal and nitrogen sublattices have two and one enlarged *d*-spacings of (0002) planes, respectively. Since strain is defined on the basis of the deformation of the unit cell, the local increase in a single *d*-spacing of the nitrogen sublattice is masked due to averaging. In the case of the metal sublattice, the peak value in Figure 6b corresponds to the *c*-spacing that contains the quantum well. For the nitrogen sublattice, two *c*-spacings are strongly affected, i.e., that one and the one above it, as shown in Figure 6b.

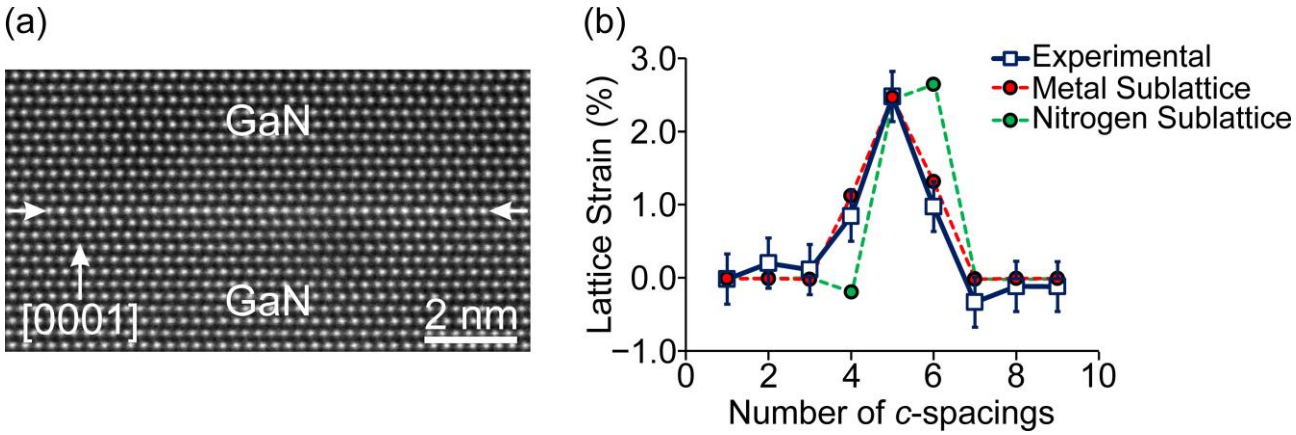

Figure 6. (**a**) HRSTEM image of 1 ML $In_xGa_{1-x}N$/GaN quantum well with indium content close to 30%. (**b**) Profiles of lattice strain e_{zz} along [0001]. Experimental profile, obtained from (**a**) by peak finding, is superimposed on calculated profiles for the metal and nitrogen sublattices for x = 33%.

Since the strain state of the superlattice is rather complex, comprising strains of opposite signs, i.e., tensing the GaN barriers reduces the strain in the quantum wells, we have considered the excess energy of the supercells as an appropriate measure to appreciate its influence on the band gap. The excess energy E_{ex} of each supercell was defined with reference to the respective energies E_{GaN} of the barriers and E_{InGaN} of the quantum wells, as expressed by the equation $E_{ex} = E_t - E_{GaN} - E_{InGaN}$, where E_t is the total energy of

the supercell. The terms E_{GaN} and E_{InGaN} were obtained from relaxed supercells. We can consider E_{ex} to comprise two contributions: one attributed to the long-range elastic strain and one due to the local interfacial interactions at the quantum wells. Figure 7a shows the variation of E_{ex} with composition, whereby the energy is normalized per atomic column along [0001]. As expected, the energy increases by increasing the indium composition. The local minimum at 33% indium is attributed to its low-energy structure [36]. The excess energies appear rather similar for 0% and 1.5% barrier strain, which should be attributed to the reduction of the compressive strain in the quantum wells when the barriers are strained by 1.5%. We note that, since the period of the superlattice is much larger than the distorted area in the quantum well region, the excess energy does not depend on the superlattice period, i.e., as long as the considered barrier width is greater than this affected region, the aforementioned arguments are valid since the term E_{GaN} incorporates any changes of the period of the superlattice.

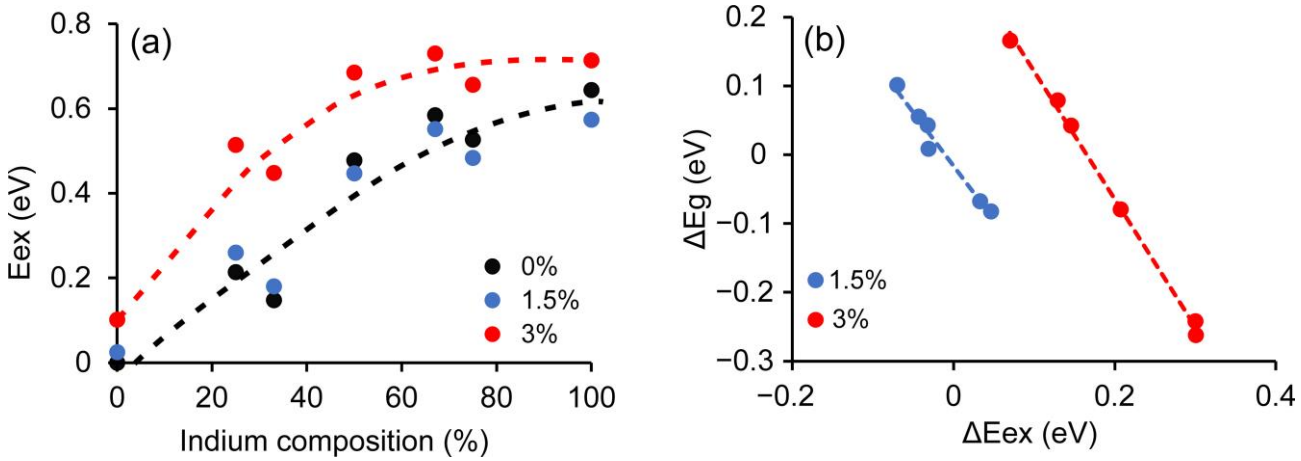

Figure 7. (**a**) Graph of excess energy of studied supercells with respect to quantum well indium content. Trendlines are guides to the eye. (**b**) Graph of band-gap energy change ΔE_g against the change in excess energy ΔE_{ex}, with reference to the superlattices with relaxed GaN barriers.

In Figure 7b, the change in the band gap ΔE_g compared with superlattices with relaxed barriers is plotted against the respective change in excess energy ΔE_{ex}. Clear linear relationships are again observed for both the 1.5% and 3% cases, which is expected since ΔE_{ex} was also a linear function of the quantum well composition. The linear behavior of ΔE_{ex} indicates that the interfacial contribution is almost constant and independent of the strain (so it cancels out), and ΔE_{ex} is mainly influenced by the long-range strain.

4. Conclusions

Using DFT calculations, we have studied, across the whole compositional range, the influence of strained GaN barriers or substrates on the band-gap energies of short-period superlattices comprising $In_xGa_{1-x}N$ quantum wells. The use of strained substrates and pseudo-substrates has been suggested in the literature for overcoming the problem of lattice misfit to increase the indium incorporation without defect introduction. Our calculations have shown that superlattices with strained GaN barriers exhibit smaller band gaps compared with those with unstrained ones but only for indium contents up to approximately 50%, since this trend is reversed for higher indium concentrations. This behavior is attributed to the interplay between the tensile in-plane strain in the barriers and the compressive strain in the quantum wells, which mainly affects the nitrogen sublattice. On the other hand, clusters of InN on the quantum well plane do not modify the behavior of the superlattice heterostructure to a significant extent compared with quantum wells with homogeneous structures. We consider that these findings provide physical insight on the influence of strain on band-gap variation and are technologically important toward an

appropriate deployment of strained substrates for band-gap engineering in these advanced superlattice heterostructures. Further calculations are needed to appreciate the efficiency of electron–hole recombination in such superlattices.

Supplementary Materials: The following supporting information can be downloaded at: https://www.mdpi.com/article/10.3390/cryst13040700/s1, Figure S1: Calculated equilibrium lattice parameters of $In_xGa_{1-x}N$ bulk alloys with respect to indium composition. A linear behavior is observed in line with Vegard's law. There is a slight deviation in the *c*-parameter of $In_{33}Ga_{67}N$ and $In_{67}Ga_{33}N$ equal to ~−0.03 Å; Figure S2: (a) Calculated band gap versus indium composition of the $In_xGa_{1-x}N$ alloys showing bowing consistent with a bowing parameter of $b = 1.18 \pm 0.09$ eV, (b) Total energy of the $In_xGa_{1-x}N$ supercells per atomic column with respect to alloy composition; Figure S3: (a) Critical thickness of GaN with respect to the in-plane strain obtained using the model of Fischer et al. [33]. The formation of elastically strained GaN barriers with thickness at least 10 MLs is permitted for in-plane strain values up to ~4%. (b): Band-gap variation of 1InN/*n*GaN short-period superlattices as a function of GaN barrier thickness *n* (unstrained barrier). The dependence of the band-gap energy on the barrier thickness is negligible for GaN barriers thicker than 7 MLs; Figure S4: Calculated lattice strain with respect to the indium content for ordered, disordered, and clustered $In_xGa_{1-x}N$/GaN quantum wells of one monolayer thickness. The plotted lattice strain is the reduced relative variation of the *c*-lattice constant along [0001] having as reference the *c*-lattice constant of GaN. The disordered quantum wells were obtained from empirical potential calculations as described elsewhere [17]. The ordered and clustered quantum wells were obtained by both empirical potential and DFT calculations.

Author Contributions: Conceptualization, P.C., I.G.V., T.K. and G.P.D.; methodology, T.K. and P.K.; validation, T.K., P.K. and V.P.; formal analysis, P.C., I.G.V., P.K. and T.K.; investigation, P.C., I.G.V., P.K. and T.K.; resources, T.K.; data curation, P.K. and V.P.; writing—original draft preparation, P.C., I.G.V. and G.P.D.; writing—review and editing, T.K., P.K. and V.P.; visualization, P.C., T.K., I.G.V. and G.P.D.; supervision, G.P.D.; project administration, T.K. and G.P.D.; funding acquisition, P.K., I.G.V. and G.P.D. All authors have read and agreed to the published version of the manuscript.

Funding: Work supported by project "INNOVATION-EL" (MIS 5002772), funded by the Operational Programme "Competitiveness, Entrepreneurship and Innovation" (NSRF 2014–2020), co-financed by Greece and the EU (European Regional Development Fund). I.G.V. acknowledges support by the State Scholarships Foundation (IKY) project "Strengthening Human Resources Research Potential via Doctorate Research" (MIS-5000432).

Institutional Review Board Statement: Not applicable.

Informed Consent Statement: Not applicable.

Data Availability Statement: The data presented in this study are available on request from the corresponding author.

Acknowledgments: We would like to thank the Aristotle University of Thessaloniki HPC infrastructure for the provision of computing resources.

Conflicts of Interest: The authors declare no conflict of interest.

References

1. Gorczyca, I.; Suski, T.; Christensen, N.E.; Svane, A. Theoretical study of nitride short period superlattices. *J. Phys. Condens. Matter* **2018**, *30*, 063001. [CrossRef] [PubMed]
2. Gorczyca, I.; Suski, T.; Strak, P.; Staszczak, G.; Christensen, N.E. Band gap engineering of In(Ga)N/GaN short period superlattices. *Sci. Rep.* **2017**, *7*, 16055. [CrossRef] [PubMed]
3. Sun, W.; Tan, C.-K.; Tansu, N. III-Nitride Digital Alloy: Electronics and optoelectronics properties of the InN/GaN ultra-short period superlattice nanostructures. *Sci. Rep.* **2017**, *7*, 6671. [CrossRef] [PubMed]
4. Kioseoglou, J.; Komninou, P.; Chen, J.; Nouet, G.; Kalesaki, E.; Karakostas, T. Structural and electronic properties of elastically strained InN/GaN quantum well multilayer heterostructures. *Phys. Status Solidi C* **2014**, *11*, 289–292. [CrossRef]
5. Ribeiro, M.; Marques, M. Theoretical study of InN/GaN short period superlattices to mimic disordered alloys. *J. Appl. Phys.* **2014**, *115*, 223708. [CrossRef]

6. Ambacher, O.; Majewski, J.; Miskys, C.; Link, A.; Hermann, M.; Eickhoff, M.; Stutzmann, M.; Bernardini, F.; Fiorentini, V.; Tilak, V.; et al. Pyroelectric properties of Al(In)GaN/GaN hetero- and quantum well structures. *J. Phys. Condens. Matter* **2002**, *14*, 3399–3434. [CrossRef]
7. Miao, M.S.; Yan, Q.; Van de Walle, C.G.; Lou, W.K.; Li, L.L.; Chang, K. Polarization-driven topological insulator transition in a GaN/InN/GaN quantum well. *Phys. Rev. Lett.* **2012**, *109*, 186803. [CrossRef]
8. Łepkowski, S.P.; Bardyszewski, W. Topological insulator with negative spin-orbit coupling and transition between Weyl and Dirac semimetals in InGaN-based quantum wells. *Sci. Rep.* **2018**, *8*, 15403. [CrossRef]
9. Pan, W.; Dimakis, E.; Wang, G.T.; Moustakas, T.D.; Tsui, D.C. Two-dimensional electron gas in monolayer InN quantum wells. *Appl. Phys. Lett.* **2014**, *105*, 213503. [CrossRef]
10. Yoshikawa, A.; Kusakabe, K.; Hashimoto, N.; Hwang, E.-S.; Itoi, T. Dynamic atomic layer epitaxy of InN on/in +c-GaN matrix: Effect of "In+N" coverage and capping timing by GaN layer on effective InN thickness. *Appl. Phys. Lett.* **2016**, *108*, 022108. [CrossRef]
11. Kusakabe, K.; Hashimoto, N.; Itoi, T.; Wang, K.; Imai, D.; Yoshikawa, A. Growth kinetics and structural perfection of $(InN)_1/(GaN)_{1–20}$ short-period superlattices on +c-GaN template in dynamic atomic layer epitaxy. *Appl. Phys. Lett.* **2016**, *108*, 152107. [CrossRef]
12. Suski, T.; Schulz, T.; Albrecht, M.; Wang, X.Q.; Gorczyca, I.; Skrobas, K.; Christensen, N.E.; Svane, A. The discrepancies between theory and experiment in the optical emission of monolayer In(Ga)N quantum wells revisited by transmission electron microscopy. *Appl. Phys. Lett.* **2014**, *104*, 182103. [CrossRef]
13. Chèze, C.; Feix, F.; Anikeeva, M.; Schulz, T.; Albrecht, M.; Riechert, H.; Brandt, O.; Calarco, R. In/GaN(0001)-$(\sqrt{3}\times\sqrt{3})$R30° adsorbate structure as a template for embedded (In, Ga)N/GaN monolayers and short-period superlattices. *Appl. Phys. Lett.* **2017**, *110*, 072104. [CrossRef]
14. Ma, D.; Rong, X.; Zheng, X.; Wang, W.; Wang, P.; Schulz, T.; Albrecht, M.; Metzner, S.; Müller, M.; August, O.; et al. Exciton emission of quasi-2D InGaN in GaN matrix grown by molecular beam epitaxy. *Sci. Rep.* **2014**, *7*, 46420. [CrossRef]
15. Dimitrakopulos, G.P.; Vasileiadis, I.G.; Bazioti, C.; Smalc-Koziorowska, J.; Kret, S.; Dimakis, E.; Florini, N.; Kehagias, T.; Suski, T.; Karakostas, T.; et al. Compositional and strain analysis of In(Ga)N/GaN short period superlattices. *J. Appl. Phys.* **2018**, *123*, 024304. [CrossRef]
16. Yoshikawa, A.; Kusakabe, K.; Hashimoto, N.; Hwang, E.-S.; Imai, D.; Itoi, T. Systematic study on dynamic atomic layer epitaxy of InN on/in +c-GaN matrix and fabrication of fine-structure InN/GaN quantum wells: Role of high growth temperature. *J. Appl. Phys.* **2016**, *120*, 225303. [CrossRef]
17. Vasileiadis, I.G.; Lymperakis, L.; Adikimenakis, A.; Gkotinakos, A.; Devulapalli, V.; Liebscher, C.H.; Androulidaki, M.; Hübner, R.; Karakostas, T.; Georgakilas, A.; et al. Substitutional synthesis of sub-nanometer InGaN/GaN quantum wells with high indium content. *Sci. Rep.* **2021**, *11*, 20606. [CrossRef]
18. Lymperakis, L.; Schulz, T.; Freysoldt, C.; Anikeeva, M.; Chen, Z.; Zheng, X.; Shen, B.; Cheze, C.; Siekacz, M.; Wang, X.Q.; et al. Elastically frustrated rehybridization: Origin of chemical order and compositional limits in InGaN quantum wells. *Phys. Rev. Materials* **2018**, *2*, 011601(R). [CrossRef]
19. Even, A.; Laval, G.; Ledoux, O.; Ferret, P.; Sotta, D.; Guiot, E.; Levy, F.; Robin, I.C.; Dussaigne, A. Enhanced In incorporation in full InGaN heterostructure grown on relaxed InGaN pseudo-substrate. *Appl. Phys. Lett.* **2017**, *110*, 262103. [CrossRef]
20. Pasayat, S.S.; Gupta, C.; Wong, M.S.; Wang, Y.; Nakamura, S.; Denbaars, S.P.; Keller, S.; Mishra, U.K. Growth of strain-relaxed InGaN on micrometer-sized patterned compliant GaN pseudo-substrates. *Appl. Phys. Lett.* **2020**, *116*, 111101. [CrossRef]
21. Abdelhamid, M.; Routh, E.L.; Hagar, B.; Bedair, S.M. Improved LED output power and external quantum efficiency using InGaN templates. *Appl. Phys. Lett.* **2022**, *120*, 081104. [CrossRef]
22. Dimitrakopulos, G.P.; Bazioti, C.; Grym, J.; Gladkov, P.; Hulicius, E.; Pangrác, J.; Pacherová, O.; Komninou, P. Misfit dislocation reduction in InGaAs epilayers grown on porous GaAs substrates. *Appl. Surface Sci.* **2014**, *306*, 89. [CrossRef]
23. Schulz, T.; Lymperakis, L.; Anikeeva, M.; Siekacz, M.; Wolny, P.; Markurt, T.; Albrecht, M. Influence of strain on the indium incorporation in (0001) GaN. *Phys. Rev. Mater.* **2020**, *4*, 073404. [CrossRef]
24. Ho, I.H.; Stringfellow, G.B. Solid phase immiscibility in GaInN. *Appl. Phys. Lett.* **1996**, *69*, 2701–2703. [CrossRef]
25. Giannozzi, P.; Baroni, S.; Bonini, N.; Calandra, M.; Car, R.; Cavazzoni, C.; Ceresoli, D.; Chiarotti, G.L.; Cococcioni, M.; Dabo, I.; et al. QUANTUM ESPRESSO: A modular and open-source software project for quantum simulations of materials. *J. Phys. Condens. Matter* **2009**, *21*, 395502. [CrossRef]
26. Giannozzi, P.; Andreussi, O.; Brumme, T.; Bunau, O.; Buongiorno Nardelli, M.; Calandra, M.; Car, R.; Cavazzoni, C.; Ceresoli, D.; Cococcioni, M.; et al. Advanced capabilities for materials modelling with QUANTUM ESPRESSO. *J. Phys. Condens. Matter* **2017**, *29*, 465901. [CrossRef]
27. Segev, D.; Janotti, A.; Van de Walle, C.G. Self-consistent band-gap corrections in density functional theory using modified pseudopotentials. *Phys. Rev. B* **2007**, *75*, 035201. [CrossRef]
28. Fletcher, R. *Practical Methods of Optimization*, 2nd ed.; John Wiley & Sons: New York, NY, USA, 1987.
29. Kazazis, S.A.; Papadomanolaki, E.; Androulidaki, M.; Kayambaki, M.; Iliopoulos, E. Optical properties of InGaN thin films in the entire composition range. *J. Appl. Phys.* **2018**, *123*, 125101. [CrossRef]
30. Moses, P.G.; Van de Walle, C.G. Band bowing and band alignment in InGaN alloys. *Appl. Phys. Lett.* **2010**, *96*, 021908. [CrossRef]

31. Duan, Y.; Qin, L.; Shi, L.; Tang, G.; Shi, H. Hybrid density functional theory study of band gap tuning in AlN and GaN through equibiaxial strains. *Appl. Phys. Lett.* **2012**, *100*, 022104. [CrossRef]
32. Namir, O.; Kioseoglou, J.; Komninou, P.; Karakostas, T.; Belabbas, I. Large out-of-plane piezoelectric response of wurtzite InN under biaxial strain. *Model. Simul. Mater. Sci. Eng.* **2021**, *29*, 065013. [CrossRef]
33. Fischer, A.; Kühne, H.; Richter, H. New Approach in Equilibrium Theory for Strained Layer Relaxation. *Phys. Rev. Lett.* **1994**, *73*, 2712–2715. [CrossRef] [PubMed]
34. Gorczyca, I.; Staszczak, G.; Targowski, G.; Grzanka, E.; Smalc-Koziorowska, J.; Suski, T.; Kawamura, T.; Kangawa, Y. Band gap tuning in $In_xGa_{1-x}N/In_yGa_{1-y}N$ short period superlattices. *Superlattices Microstruct.* **2021**, *155*, 106907. [CrossRef]
35. Gorczyca, I.; Łepkowski, S.P.; Suski, T.; Christensen, N.E.; Svane, A. Influence of indium clustering on the band structure of semiconducting ternary and quaternary nitride alloys. *Phys. Rev. B* **2009**, *80*, 075202. [CrossRef]
36. Lee, S.; Freysoldt, C.; Neugebauer, J. Ordering phenomena and formation of nanostructures in $In_xGa_{1-x}N$ layers coherently grown on GaN(0001). *Phys. Rev. B* **2014**, *90*, 245301. [CrossRef]